

Aluminum vacancy/sulfur complex in wurtzite AlN as an optically controllable spin qubit

Sergey Stolbov^{1,*} and Marisol Alcántara Ortigoza²¹Physics Department, University of Central Florida, Orlando, Florida 32816, USA²Physics Department, Tuskegee University, Tuskegee Institute, Alabama, USA

(Received 15 February 2024; accepted 22 May 2024; published 7 June 2024)

Using our rational methodology, we reveal a defect in wurtzite AlN that can serve as an optically controllable spin qubit. It combines an Al vacancy and a S atom substituting the neighboring N atom ($V_{\text{Al}}\text{S}_{\text{N}}$). Linear response *GW* and Bethe-Salpeter equation calculations guide us to find suitable ground and excited triplet and singlet states of $V_{\text{Al}}\text{S}_{\text{N}}$. The obtained optical spin-polarization cycle is similar to that observed in the negative nitrogen-vacancy (NV^-) center in diamond. The calculated optical oscillator strengths for $V_{\text{Al}}\text{S}_{\text{N}}$ suggest that, in contrast to the NV^- center, the optical emission in the singlet and triplet states have comparable rates, which is favorable for the qubit functionality.

DOI: [10.1103/PhysRevB.109.L241108](https://doi.org/10.1103/PhysRevB.109.L241108)

Quantum bits (qubits) are the key building blocks for quantum computing applications. Among several known types of qubits, spin qubits have some advantages such as long coherence time, possible room-temperature operability, and compatibility with silicon technologies. In this work we focus on optically controllable spin qubits, in which optical transitions are utilized for readout and qubit manipulation.

The properties required for spin qubits can be achieved via local defects in semiconductors. The optical readout and manipulation of a spin qubit are complex processes requiring a combination of several specific properties of the defect. It is thus not surprising that for the first and most studied spin qubit defect—the negatively charged nitrogen-vacancy center in diamond (NV^- center)—it took about two decades to detect its charged nature [1], to demonstrate a feasible preparation-readout qubit (or spin-polarization) cycle [2,3], to describe its electronic structure [4–6], and to formulate a consistent theoretical description of its entire cycle [7,8]. Thus, understanding the NV^- center properties is a basis for rational design of new defect-based qubits. The NV^- center combines a C vacancy and a N atom substituting the C atom next to the vacancy. Here are the essential properties of this defect for the spin qubit functionality: (a) it has a triplet lowest-energy ground state (TGS) with spin projections $m_s = 0$ and ± 1 , which are split due to the electron spin-spin interaction; (b) it has a local minimum singlet ground state (SGS) of higher energy; (c) an optical transition from the TGS to an excited triplet state (TES) changes the electron charge distribution leading to a phonon-assisted transition toward an excited singlet state (SES); (d) the TES-SES transition is phonon mediated and changes the spin state. This transition is possible because the spin-orbit coupling affords conservation of total angular momentum and must obey selection rules determined by the symmetry of both the TES and the SES [4,5,9], which allow transitions from the TES only for spin projections

$m_s = \pm 1$ (intersystem crossing) [10,11]. (e) An optical SES-SGS emission is available [12]; (f) phonon-assisted decay from a SGS to a TGS is feasible; (g) the electronic states associated with the above transitions are localized within the host band gap ensuring a long coherence time. These properties make possible the so-called optical spin-polarization cycle: An optical excitation from a TGS to a TES is followed by two possible processes: (1) an optical emission back to a TGS and (2) a nonradiative transition to a SES. The latter transition is only allowed for the triplet excited $m_s = \pm 1$ states due to the above-mentioned selection rules. Next, an optical SES-SGS emission occurs, followed by another nonradiative transition from a SGS to a TGS. Consequently, this cycle results in the dominating $m_s = 0$ spin polarization of a TGS necessary for initialization and readout of the qubit [8].

Other widely discussed defects with spin-qubit properties are a neutral silicon-carbon divacancy and a negatively charged silicon vacancy in SiC polytypes [13,14]. The electronic structures of these SiC defects differ from each other and from that of the NV^- center. For example, in contrast to the NV^- center, the silicon vacancy defect has a ground state with spin = 3/2. However, the optical spin-polarization cycles are all similar to that of the NV^- center. The above-described cycling steps of the NV^- center can thus serve as a recipe to evaluate new optically controllable spin qubits.

Although some guidelines have been proposed to design qubits [15,16], the NV^- and SiC-based defects are the only known systems having promising spin qubit properties, and yet they are not free of disadvantages, such as technological difficulties implementing the NV^- centers in diamond. Thus, finding new efficient spin-qubit defects is of critical importance. Wurtzite AlN (wAlN) is a propitious qubit host because it is a wide band gap semiconductor (~ 6 eV). And yet, first-principles calculations for an Al vacancy (V_{Al}) in wAlN [17,18] and for a neutral defect combining an Al vacancy and O atom substituting N next to the vacancy ($V_{\text{Al}}\text{O}_{\text{N}}$) [19] show that some defect states associated with formation of the triplet state reside inside of the valence band (VB),

*Contact author: sergey.stolbov@ucf.edu

which is unfavorable for qubit functionality. Nevertheless, these results do not signify that wAlN is an unsuitable host for defect-based qubits since (1) uniaxial strain applied to V_{Al} in wAlN significantly improves the energy diagram [18], but more importantly, (2) *the energetic position of the defect states depends not only on the host but also on the dopant properties*. This dependence has also been discussed in Ref. [16]. Hence, here we rationally explore dopants that could render wAlN an efficient optically controllable spin qubit host.

We selected a neutral defect in wAlN combining an Al vacancy and a S atom substituting the N next to the vacancy ($V_{\text{Al}}\text{S}_{\text{N}}$) and evaluated its spin-qubit related properties from first principles. Our design is based on the following reasoning: Removal of an Al atom decreases the even number of p electrons by 1, while the replacement of N with S brings back one electron making the number of p electrons even again, which is necessary for triplet formation. Moreover, the vacancy creates three N dangling bonds, which is beneficial for spin polarization. The relatively low electronegativity of S hints that it will not bind as strongly as O, possibly shifting the defect states to the band gap. We also expected that this defect will have C_{3v} symmetry as the NV^- center does, which is favorable for the spin-polarization cycle. Regarding stability of this defect, as shown in Ref. [20], an Al vacancy in AlN would tend to become negatively charged, because of the loss of the valence electrons donated by Al to bind with N. In turn, substitution of N by chalcogen atoms, such as O or S, adds an extra electron to the system. Thus, the combined presence of the Al vacancy and S (or O in Ref. [20]) seems to stabilize the neutral $V_{\text{Al}}\text{S}_{\text{N}}$ defect in AlN. The next step in our methodology is as follows: First, we use first-principle calculations to reveal whether the defect has a TGS associated with defect states. If so, we evaluate its stability by calculating the defect's formation energy and phonon spectrum. Then, we obtain the defect's electronic structure and optical excitation characteristics. If they are favorable for qubit functionality, we search for a SGS state and evaluate its stability, electronic structure, and optical properties. Finally, we build the energy diagram associated with the optical spin-polarization cycle to assess its qubit functionality.

All calculations in this work have been performed using the Vienna *Ab initio* Simulation Package VASP5.4 [21] with the projector-augmented-wave potentials [22]. For all calculations we used a 400-eV cutoff energy for the plane-wave expansion. For ground-state calculations, such as formation energies and phonon spectra, we applied the density functional theory (DFT) based Perdew-Burke-Ernzerhof (PBE) approximation for the exchange and correlation functional [23]. These calculations were performed for a $4 \times 4 \times 3$ supercell including 192 atoms with the $3 \times 3 \times 2$ k -point sampling in the Brillouin zone. The electronic structure, in terms of the independent quasiparticle (IQP) states, was calculated using the self consistent *GW* method [24] with three electronic iterations. Optical excitation characteristics such as frequency-dependent dielectric functions and oscillator strengths were calculated by solving the Bethe-Salpeter equation (BSE) using the wave functions and kernels obtained within *GW* as input [25]. Since the *GW* method is time consuming, for the *GW*-BSE calculations we use a $3 \times 3 \times 2$ supercell with 72 atoms. In this case, we used

a $4 \times 4 \times 3$ k -point mesh in the Brillouin zone. Note that such combination of computational methods has rendered a reliable description of stability, electronic structure, and optical properties of local defects in semiconductors [26,27].

The $V_{\text{Al}}\text{S}_{\text{N}}$ defect was constructed via removal of Al and substitution of N with S in the pristine wAlN structure. Interestingly, the triplet polarization was obtained even before lattice relaxation. The relaxed structures of both the $3 \times 3 \times 2$ and $4 \times 4 \times 3$ supercells render a triplet state with C_{3v} symmetry. The defect formation energies are 4.78 and 4.72 eV for the N-rich and N-poor conditions, respectively. These values are comparable or lower than those obtained for the NV^- center (4–6 eV, depending on the Fermi level position, E_{F} [3]), and much lower than that reported for neutral $V_{\text{Al}}\text{O}_{\text{N}}$ (7 eV) [19]. The phonon spectrum at the Γ point indicates that the structure of $V_{\text{Al}}\text{S}_{\text{N}}$ in wAlN is dynamically stable.

The *GW* electronic structure of the $V_{\text{Al}}\text{S}_{\text{N}}$ defect in the triplet state is found to be promising for spin qubit functionality. Indeed, as shown in the left panel of Fig. 1, the four electrons determining the TGS in $V_{\text{Al}}\text{S}_{\text{N}}$ occupy narrow *GW* IQP peaks located in the band gap. The spin density (right panel of Fig. 1) is evenly distributed among three dangling bonds associated with the three N atoms next to the vacancy, yielding a total magnetization per supercell of $2.0 \mu_{\text{B}}$. The spin density lobes are directed toward the vacancy reflecting sp^3 hybridization, which is very similar to the NV^- center case [6,28]. The optical excitation spectrum of the triplet $V_{\text{Al}}\text{S}_{\text{N}}$ obtained from BSE calculations is shown in the left panel of Fig. 2. The excitations are represented by numerous BSE eigenstates grouped between 1.0 and 1.2 eV. It is worth mentioning that, in contrast to the NV^- center triplet excitation, this one is not in the visible but in the near-infrared region.

The next step is to find a singlet state which results from the structural transformation the TES undergoes. To locate the singlet state, we designed the following method: First, we evaluated the changes in electron charge density caused by the optical excitation in the triplet. To this end, we revealed the *GW* IQP bands which contribute the most to the BSE eigenstate associated with the largest oscillator strength of the excitations at ~ 1.2 eV (left panel of Fig. 2). More specifically, we obtained changes in the local valence charges within the Wigner-Seitz spheres (Q_{WS}) when an electron moves from the corresponding initial to final IQP states. We found that marked changes in Q_{WS} occurred only in the three N atoms next to the vacancy (we label them as N_1, N_2, N_3). Yet, the changes are not even: while $Q_{\text{WS}}(N_1)$ increases by $0.10e$, $Q_{\text{WS}}(N_2)$ and $Q_{\text{WS}}(N_3)$ decrease by $0.04e$. The charge density redistribution upon excitation in the triplet reduces its symmetry to C_1 and is expected to trigger a change in the geometric structure of the system. Noticeably, it has been suggested that the TES of the NV^- center also has C_1 symmetry [29]. To mimic the possible lattice reaction to the above charge redistribution, we assumed that a decrease in the Q_{WS} of the N atoms causes a decrease in bond length between the corresponding N atom and its neighboring Al atoms, while an increase in Q_{WS} induces an increase in the corresponding N-Al bond lengths. In other words, we assumed that N_1 moves toward the vacancy, while N_2 and N_3 move away from the vacancy. We apply this reasoning to distort the TGS lattice according to the expected reaction on the charge redistribution as follows. Specifically,

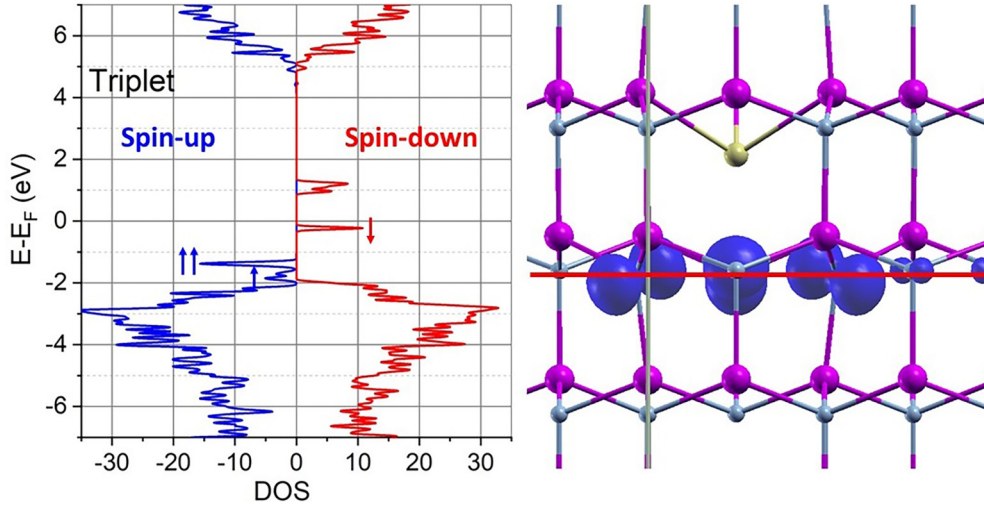


FIG. 1. Left panel: Densities of the IQP states calculated for the triplet state of the $V_{Al}S_N$ defect using the self-consistent GW method. The arrows represent the four up and down spin occupied states of the defect. Right panel: The spin density isosurface (dark blue) calculated for the triplet state of the $V_{Al}S_N$ defect. The purple, grey, and yellow balls represent Al, N, and S atoms, respectively. The red line indicates the plane passing through the centers of the three N atoms next to the vacancy.

we moved N_2 and N_3 away from the vacancy by 0.04 \AA and the N_1 atom toward the vacancy by 0.06 \AA . Indeed, structural relaxation of this configuration yielded a SGS. It is worth noticing that for some specific initial spin configurations of the distorted lattice the structural relaxation brings the system back to the TGS. This reflects the fact that the distorted structure is tailored based on an educated guess, and is not the actual TES but hopefully a state along or close to the path of the structural response to the optical excitation and does not correspond to a local minimum energy state. The details of the relaxation process show that the specific *a priori* displacements (0.04 and 0.06 \AA) imposed on the lattice do put the system in some intermediate transition state which is naturally sensitive to variations of the system's parameters, such as spin

configuration. Nevertheless, the distorted structure easily relaxes to the SGS for most initial spin configurations. The total energy of this SGS is 0.053 eV higher than that of the TGS. The obtained SGS is thus a local minimum of the potential energy surface. The calculated phonon spectrum indicated that the SGS structure is also dynamically stable.

The calculated density of the GW IQP states of the SGS is displayed in the left panel of Fig. 3. It shows that one of the electrons determining the spin state of the defect occupies an IQP peak aligned with the top of the VB, while the three others occupy local narrow peaks located in the band gap. In the SGS, the charge density of N_1 , N_2 , and N_3 are not even: while $Q_{WS}(N_2)=Q_{WS}(N_3)$, $Q_{WS}(N_1) < Q_{WS}(N_{2,3})$ by $0.07e$. Interestingly, although it is a singlet (total magnetization per

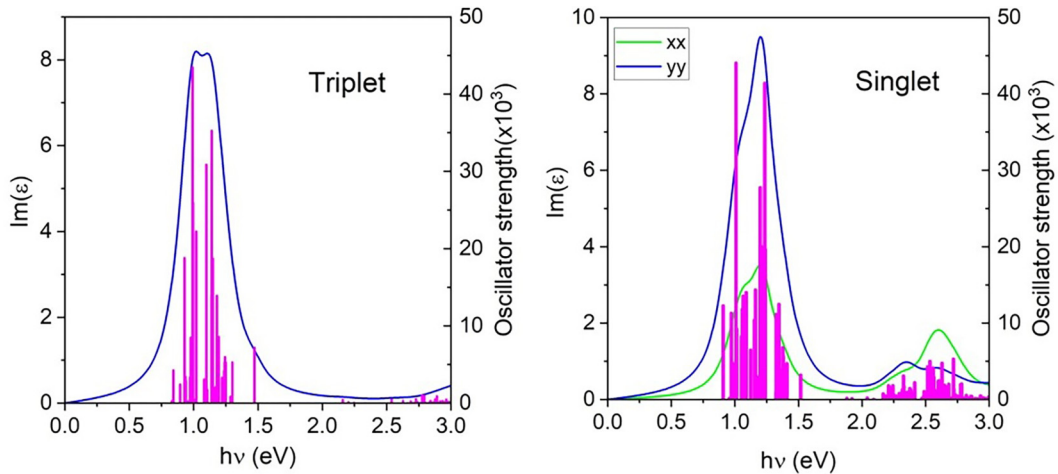


FIG. 2. The frequency-dependent dielectric function (blue and green lines) and the oscillator strength (pink bars) calculated for the triplet (left panel) and singlet (right panel) states in $V_{Al}S_N$ defect in wAlN. For both, the zz polarization makes a negligible contribution to $\text{Im}(\epsilon)$. For the triplet, the xx and yy polarizations are degenerated. The main contribution to the excitation at 1.2 eV for the triplet comes from transitions among IQP states located along the $\Gamma - K$ and $\Gamma - M$ directions in the Brillouin zone. For the singlet, the main contribution to the BSE eigenstates associated to the excitation at 1.0 eV comes from transitions among IQP states located along the $\Gamma - K$ directions in the Brillouin zone.

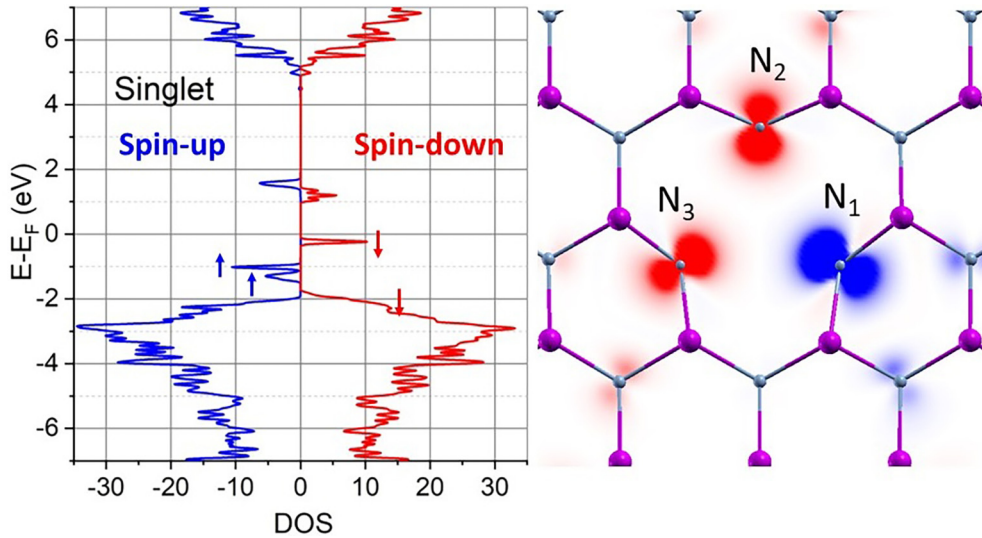


FIG. 3. Left panel: Densities of the IQP states calculated for the GS of the $V_{\text{Al}}\text{S}_\text{N}$ defect using the self-consistent GW method. Right panel: A cut of the spin density along the plane passing by $N_{1,2,3}$, shown as a red line in Fig. 1. Spin-up and spin-down densities are represented by blue and red areas, respectively. The purple and grey balls represent Al and N atoms, respectively.

supercell equals zero), the spin density on N_1 , N_2 , and N_3 individually is not zero (right panel of Fig. 3). The integrated spin density within the Wigner-Seitz spheres (S_{WS}) shows that the spin-up and $S_{\text{WS}}(N_1)$ is approximately two times larger in magnitude than the spin-down $S_{\text{WS}}(N_2)$ and $S_{\text{WS}}(N_3)$. Thus, the system in the SGS has C_1 symmetry. Since the $V_{\text{Al}}\text{S}_\text{N}$ TGS has C_{3v} symmetry, it can be transformed into three identical SGSs, one of which has been described above. We obtained the other two singlets with the same total energy and the geometry rotated by 120° with respect to each other.

Since the energy difference between the TES and the SGS is large (~ 0.9 to ~ 1.1 eV) compared to the phonon energies of the system, a direct nonradiative phonon-induced transition from the former to the latter is unlikely. Thus, some intermediate SES state may be needed. To find such a state, we calculated the optical excitation spectrum for the singlet using the BSE method. The spectrum characteristics are shown in the right panel of Fig. 2. In contrast to the triplet spectrum, the xx and yy polarizations of $\text{Im}(\epsilon)$ are not degenerated, reflecting the reduced symmetry of the system. It is worth mentioning that according to our analysis of the excitation effect on Q_{WS} , the SES still retains the C_1 symmetry. The spectrum is divided in two distinct energy groups. The lower energy excitation group is between 0.9 and 1.4 eV and all corresponding excitations originate from the spin-down states (left panel of Fig. 3). The higher energy excitation group (2.2–2.8 eV) results from transitions between the spin-up states. The lower energy excited state may serve as an intermediate state in the path of the spin-selective decay of the spin-polarization cycle. Remarkably, the oscillator strength for the singlet excitation is practically the same as that for the triplet. We must mention that, for the NV^- center, the experimental zero-phonon line intensity of the singlet state is four orders of magnitude lower than that of the triplet [12]. This fact has been attached in part to the specifics of the phonon spectrum of the SGS [7]. Nevertheless, the phonon

influence will not make a difference of four orders of magnitude under any circumstances. Thus, the oscillator strength remains one of the main factors determining the emission rate of the singlet. Therefore, our above-mentioned results on the oscillator strength suggest that, in contrast to the NV^- center in diamond, the intensity of the emission for the singlet and triplet in $V_{\text{Al}}\text{S}_\text{N}$ will be comparable, which may be critical for an efficient spin-polarization cycle.

The next step is to model the nonradiative SGS-TGS transition. Since it would be time consuming to find the lowest energy transition path for the 191-atom system, we tried the simplest possible path made of consecutive displacements of all 191 atoms from their singlet coordinates $[\tilde{\mathbf{r}}_i(\text{singlet})]$ to their triplet ones $[\tilde{\mathbf{r}}_i(\text{triplet})]$ by a fraction x of $\tilde{\mathbf{r}}_i(\text{singlet}) - \tilde{\mathbf{r}}_i(\text{triplet})$. The coordinates of the displaced atoms, $\tilde{\mathbf{r}}_i(x)$, were thus represented by a linear combination of the singlet and triplet atom coordinates:

$$\tilde{\mathbf{r}}_i(x) = (1 - x)\tilde{\mathbf{r}}_i(\text{singlet}) - x\tilde{\mathbf{r}}_i(\text{triplet}).$$

The DFT calculations were performed for 15 coordinate shifts ($n = 15$ values of x for $0 \leq x \leq 1$) starting from the singlet configuration. For each x_n value we use the wave function obtained for the previous x_{n-1} value. In this way we obtain the transition energy barrier shown in the left panel of Fig. 4. And although this may not be the lowest energy path, our result shows that the energy barrier for the transition from the SGS to TGS is not higher than 0.15 eV, which makes the transition feasible because such barrier can be easily overcome via phonon excitations.

Finally, we built the energy diagram for the entire optical spin-polarization cycle of the $V_{\text{Al}}\text{S}_\text{N}$ defect in wAlN, which is shown in the right panel of Fig. 4. The cycle is very similar to that of the NV^- center: an optical excitation from the TGS to the TES changes the charge distribution and reduces the symmetry of the system, which leads to a presumably spin-selective phonon-assisted transition from the TES to the

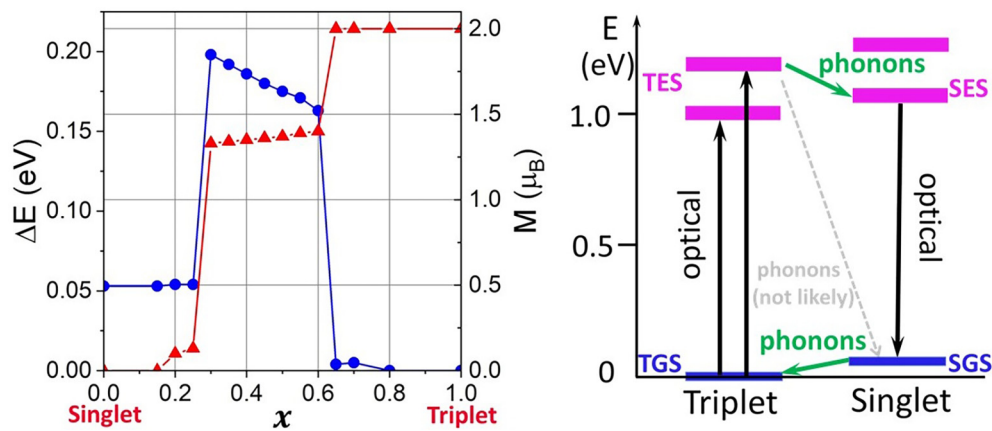


FIG. 4. Left panel: Blue line and symbols represent energy profile (with the reference to the total energy of the triplet state) of the transition path from the singlet to triplet state of the $V_{Al}S_N$ defect. The transition path as a function of x is described in the text. Red line and symbols represent the supercell magnetization along the transition path. Right panel: Energy diagram for possible triplet-singlet-triplet transformations in $V_{Al}S_N$. The dark-blue lines (TGS and SGS) and pink bands (TES and SES) represent the electronic ground and excited states of the triplet and singlet, correspondingly. The dashed (light gray) line indicates the unlikely but possible direct transition between the TES and the SGS.

SES. Next, an optical emission brings the system to SGS, followed by a nonradiative phonon-assisted transition back to the TGS.

In conclusion, based on our rational methodology, we selected the $V_{Al}S_N$ defect in wAlN and evaluated its spin qubit functionality. Our calculations reveal thermodynamically stable triplet and singlet ground states for $V_{Al}S_N$, where the triplet state has an energy 0.053 eV lower than the singlet one. Using the *GW*-BSE methods we calculate the electronic structure and optical excitations for both the triplet and singlet states of the $V_{Al}S_N$ defect in wAlN. Using these results we build the energy diagram of the optical spin-polarization cycle required for initialization of the qubit. We find an energy diagram very similar to that of the NV^- center in diamond.

Importantly, our BSE calculation of the oscillator strength of the optical transition between the singlet ground and excited states suggests that this step for the $V_{Al}S_N$ defect is optically more favorable for the spin-polarization cycle than that for the NV^- diamond center. Thus, our results indicate that the $V_{Al}S_N$ defect in wAlN is a promising spin qubit as its properties are favorable for the optical spin-polarization cycle.

This work was supported by the U.S. Department of Energy, Office of Science, Basic Energy Sciences, under Award No. DE-SC0024487. The author acknowledges the University of Central Florida Advanced Research Computing Center for providing computational resources and support that have contributed to results reported herein [30].

- [1] A. Gruber, A. Drabenstedt, C. Tietz, L. Fleury, J. Wrachtrup, and C. von Borczyskowski, Scanning confocal optical microscopy and magnetic resonance on single defect centers, *Science* **276**, 2012 (1997).
- [2] F. Jelezko, T. Gaebel, I. Popa, M. Domhan, A. Gruber, and J. Wrachtrup, Observation of coherent oscillation of a single nuclear spin and realization of a two-qubit conditional quantum gate, *Phys. Rev. Lett.* **93**, 130501 (2004).
- [3] F. Jelezko, T. Gaebel, I. Popa, A. Gruber, and J. Wrachtrup, Observation of coherent oscillations in a single electron spin, *Phys. Rev. Lett.* **92**, 076401 (2004).
- [4] J. R. Maze, A. Gali, E. Togan, Y. Chu, A. Trifonov, E. Kaxiras, and M. D. Lukin, Properties of nitrogen-vacancy centers in diamond: The group theoretic approach, *New J. Phys.* **13**, 025025 (2011).
- [5] M. W. Doherty, N. B. Manson, P. Delaney, and L. C. L. Hollenberg, The negatively charged nitrogen-vacancy centre in diamond: The electronic solution, *New J. Phys.* **13**, 025019 (2011).
- [6] V. Ivády, I. A. Abrikosov, and A. Gali, First principles calculation of spin-related quantities for point defect qubit research, *npj Comput. Mater.* **4**, 76 (2018).
- [7] G. Thiering and A. Gali, Theory of the optical spin-polarization loop of the nitrogen-vacancy center in diamond, *Phys. Rev. B* **98**, 085207 (2018).
- [8] A. Gali, *Ab initio* theory of the nitrogen-vacancy center in diamond, *Nanophotonics* **8**, 1907 (2019).
- [9] M. W. Doherty, N. B. Manson, P. Delaney, F. Jelezko, J. Wrachtrup, and L. C. L. Hollenberg, The nitrogen-vacancy colour centre in diamond, *Phys. Rep.* **528**, 1 (2013).
- [10] M. L. Goldman, A. Sipahigil, M. W. Doherty, N. Y. Yao, S. D. Bennett, M. Markham, D. J. Twitchen, N. B. Manson, A. Kubanek, and M. D. Lukin, Phonon-induced population dynamics and intersystem crossing in nitrogen-vacancy centers, *Phys. Rev. Lett.* **114**, 145502 (2015).
- [11] M. L. Goldman, M. W. Doherty, A. Sipahigil, N. Y. Yao, S. D. Bennett, N. B. Manson, A. Kubanek, and M. D. Lukin, State-selective intersystem crossing in nitrogen-vacancy centers, *Phys. Rev. B* **91**, 165201 (2015).
- [12] L. J. Rogers, S. Armstrong, M. J. Sellars, and N. B. Manson, Infrared emission of the NV centre in diamond: Zeeman and uniaxial stress studies, *New J. Phys.* **10**, 103024 (2008).

- [13] W. F. Koehl, B. B. Buckley, F. J. Heremans, G. Calusine, and D. D. Awschalom, Room temperature coherent control of defect spin qubits in silicon carbide, *Nature (London)* **479**, 84 (2011).
- [14] M. Widmann, S. Y. Lee, T. Rendler *et al.*, Coherent control of single spins in silicon carbide at room temperature, *Nat. Mater.* **14**, 164 (2015).
- [15] G. Wolfowicz, F. J. Heremans, C. P. Anderson, S. Kanai, H. Seo, A. Gali, G. Galli, and D. D. Awschalom, Quantum guidelines for solid-state spin defects, *Nat. Rev. Mater.* **6**, 906 (2021).
- [16] J. R. Weber, W. F. Koehl, J. B. Varley, A. Janotti, B. B. Buckley, C. G. Van de Walle, and D. D. Awschalom, Quantum computing with defects, *Proc. Natl. Acad. Sci. USA* **107**, 8513 (2010).
- [17] Y. Gohda and A. Oshiyama, Stabilization mechanism of vacancies in Group-III nitrides: Exchange splitting and electron transfer, *J. Phys. Soc. Jpn.* **79**, 083705 (2010).
- [18] H. Seo, M. Govoni, and G. Galli, Design of defect spins in piezoelectric aluminum nitride for solid-state hybrid quantum technologies, *Sci. Rep.* **6**, 20803 (2016).
- [19] Y. Tu, Z. Tang, X. G. Zhao, Y. Chen, Z. Q. Zhu, J. H. Chu, and J. C. Fang, A paramagnetic neutral VAION center in wurtzite AlN for spin qubit application, *Appl. Phys. Lett.* **103**, 072103 (2013).
- [20] C. Stampfl and C. G. Van de Walle, Theoretical investigation of native defects, impurities, and complexes in aluminum nitride, *Phys. Rev. B* **65**, 155212 (2002).
- [21] G. Kresse and G. J. Furthmüller, Efficient iterative schemes for ab initio total-energy calculations using a plane-wave basis set, *Comput. Mater. Sci.* **6**, 15 (1996).
- [22] G. Kresse and J. Joubert, From ultrasoft pseudopotentials to the projector augmented-wave method, *Phys. Rev. B* **59**, 1758 (1999).
- [23] J. P. Perdew, S. Burke, and M. Ernzerhof, Generalized gradient approximation made simple, *Phys. Rev. Lett.* **77**, 3865 (1996).
- [24] M. Shishkin, M. Marsman, and G. Kresse, Accurate Quasiparticle spectra from self-consistent GW calculations with vertex corrections, *Phys. Rev. Lett.* **99**, 246403 (2007).
- [25] G. Onida, L. Reining, and A. Rubio, Electronic excitations: Density-functional versus many-body Green's-function approaches, *Rev. Mod. Phys.* **74**, 601 (2002).
- [26] M. Alcántara Ortigoza and S. Stolbov, Thermodynamic stability and optical properties of C-doping-induced defects in hexagonal boron nitride as potential single-photon emitters, *Phys. Rev. B* **105**, 165306 (2022).
- [27] S. Stolbov, Local defects in two-dimensional gallium sulfide, as potential single-photon emitters: First-principle evaluation, *Phys. Rev. B* **106**, 245205 (2022).
- [28] Y. Ma, M. Rohlfing, and A. Gali, Excited states of the negatively charged nitrogen-vacancy color center in diamond, *Phys. Rev. B* **81**, 041204(R) (2010).
- [29] J. Zhang, C.-Z. Wang, Z. Z. Zhu, and V. V. Dobrovitski, Vibrational modes and lattice distortion of a nitrogen-vacancy center in diamond from first-principles calculations, *Phys. Rev. B* **84**, 035211 (2011).
- [30] <https://arcc.ist.ucf.edu>